HHS Public Access

Author manuscript

Immunohorizons. Author manuscript; available in PMC 2023 September 28.

Published in final edited form as:

Immunohorizons. 2022 December 01; 6(12): 851–863. doi:10.4049/immunohorizons.2200075.

Dam-infant rhesus macaque pairs to dissect age-dependent responses to SARS-CoV-2 infection

Stephanie N. Langel[1], **Carolina Garrido**[2], **Caroline Phan**[2], **Tatianna Travieso**[2], **Helene Kirshner**[2], **Todd DeMarco**[2], **Zhong-Min Ma**[3], **J. Rachel Reader**[3], **Katherine J. Olstad**[3], **Rebecca L. Sammak**[3], **Yashavanth Shaan Lakshmanappa**[4], **Jamin W. Roh**[4,5], **Jennifer Watanabe**[3], **Jodie Usachenko**[3], **Ramya Immareddy**[3], **Rachel Pollard**[4], **Smita S. Iyer**[3,4,6], **Sallie Permar**[7], **Lisa A. Miller**[3,8], **Koen K.A. Van Rompay**[3], **Maria Blasi**[2,9]

[1] Center for Global Health and Diseases, Department of Pathology, Case Western Reserve University School of Medicine, Cleveland, Ohio, USA

[2] Duke Human Vaccine Institute, Duke University School of Medicine, Durham, NC, USA

[3] California National Primate Research Center, University of California, Davis, CA USA

[4] Center for Immunology and Infectious Diseases, University of California, Davis, CA USA

[5] Graduate Group in Immunology, UC Davis, CA

[6] Department of Pathology, Microbiology, and Immunology, School of Veterinary Medicine, UC Davis, CA

[7] New York-Presbyterian/Weill Cornell Medical Center, Department of Pediatrics, New York, NY, USA

[8] Department of Anatomy, Physiology, and Cell Biology, School of Veterinary Medicine, UC Davis, CA

[9] Department of Medicine Division of Infectious Diseases, Duke University School of Medicine, Durham, NC, USA

Abstract

The global spread of Severe Acute Respiratory Syndrome Coronavirus 2 (SARS-CoV-2) and its associated coronavirus disease (COVID-19) has led to a pandemic of unprecedented scale. An intriguing feature of the infection is the minimal disease in most children, a demographic at higher risk for other respiratory viral diseases. To investigate age-dependent effects of SARS-CoV-2

[#]Address correspondence to: Maria Blasi, maria.blasi@duke.edu.

Author contributions.

S.N.L., C.G., C.P., T.T., H.K., T.D., Z.M., J.R.R., K.J.O., R.L.S., Y.S.L., J.W.R., J.W., J.U., R.I. and R.P. performed experiments and analyzed the data, S.N.L. wrote the initial draft of the manuscript, S.N.L., S.S.I., S.P., L.A.M., K.K.A.V.R. contributed to study design, data analysis and editing of the manuscript. All authors edited the manuscript. M.B. oversaw the planning and direction of the project including analysis and interpretation of the data and editing of the manuscript

The authors have no financial conflict of interest. The funders had no role in study design, data collection and interpretation, or the decision to submit the work for publication. We thank the Duke Human Vaccine Institute (DHVI) DHVI Viral Genetics Analysis Core for their support with RNAseq.

RNAseq data accession number: PRJNA904310;

RNAseq data URL: https://www.ncbi.nlm.nih.gov/bioproject/904310

pathogenesis, we inoculated two rhesus macaque monkey dam-infant pairs with SARS-CoV-2 and conducted virological and transcriptomic analysis of the respiratory tract and evaluated systemic cytokine and antibody responses. Viral RNA levels in all sampled mucosal secretions were comparable across dam-infant pairs in the respiratory tract. Despite comparable viral loads, adult macaques showed higher IL-6 in serum at day 1 post infection while CXCL10 was induced in all animals. Both groups mounted neutralizing antibody (nAb) responses, with infants showing a more rapid induction at day 7. Transcriptome analysis of tracheal airway cells isolated at day 14 post-infection revealed significant upregulation of multiple interferon-stimulated genes in infants compared to adults. In contrast, a profibrotic transcriptomic signature with genes associated with cilia structure and function, extracellular matrix (ECM) composition and metabolism, coagulation, angiogenesis, and hypoxia was induced in adults compared to infants. Our study in rhesus macaque monkey dam-infant pairs suggests age-dependent differential airway responses to SARS-CoV-2 infection and describes a model that can be used to investigate SARS-CoV-2 pathogenesis between infants and adults.

INTRODUCTION

The epidemiological evidence has consistently demonstrated that SARS-CoV-2 infections in young children are mostly mild with relatively low hospitalization rates (1, 2). This results in significantly decreased fatality rates of young (0–9 years old) compared with old (>70-year-old) populations (3–9). Despite the increase in pediatric hospitalizations during emergence of the Delta variant, the proportion of children with severe disease after the Delta variant became predominant were similar to those earlier in the pandemic (10). This suggests that the increase in pediatric hospitalizations during this time is related to other factors, and that children are still at significantly lower risk to severe COVID-19 compared to adults.

Differences in local immune responses in the respiratory tract that include antiviral and pro-inflammatory mediators likely play a role in the age-dependent pathogenesis of SARS-CoV-2 (11). Indeed, children have increased expression of relevant pattern recognition receptors including MDA5 (*IFIH1*) and RIG-I (*DDX58*) in the upper airways when compared to adults (12), suggesting that recognition of SARS-CoV-2 entry into respiratory cells is enhanced in children. This is relevant for recruitment of fast-acting innate immune cells like neutrophils, which were shown to be higher in children during the acute phase of SARS-CoV-2 infection compared to adults (13). Interferon (IFN) responses are also key determinants of COVID-19 severity, and potent production of type III, and to a lesser extent type I IFNs in the upper respiratory tract are associated with decreased viral load, milder COVID-19 and younger age (14). However, there remains a large gap in our understanding of how age-dependent factors mediate disease severity and recovery post-infection.

Non-human primate (NHP) models are valuable resources to address these questions related to SARS-CoV-2 pathobiology and to explore vaccine and drug-based interventions against COVID-19 (15, 16). We used a maternal-infant SARS-CoV-2 infection model to elucidate the age-dependent effects on viral pathogenesis. By using dam-infant pairs and inoculating both dams and infants at the same time, we were able to simultaneously analyze immune

responses to SARS-CoV-2 infection in two different age groups while limiting genetic variation. We show that SARS-CoV-2 infection in dam-infant rhesus macaque pairs results in innate and adaptive immune differences including SARS-CoV-2 neutralizing antibody response kinetics and innate immune and profibrotic gene expression in the conducting airways. Our data highlight age-dependent differential immune and lung responses to SARS-CoV-2 infection and describes a model that can be used to investigate SARS-CoV-2 pathogenesis between infants and adults.

MATERIALS AND METHODS

Animals, SARS-CoV-2 infection and sample collection

The four Indian origin rhesus macaques (Macaca mulatta) used in this study were housed at CNRPC in accordance with the recommendations of the Association for Assessment and Accreditation of Laboratory Animal Care International Standards and with the recommendations in the Guide for the Care and Use of Laboratory Animals of the United States - National Institutes of Health (NIH). The Institutional Animal Use and Care Committee approved these experiments (study protocol# 21702). All animals were challenged through combined intratracheal (IT, 2.0 mL for dams, 1 ml for infants) and intranasal (IN, 0.2 5 mL per nostril) inoculation with an infectious dose of 2.5 × 10^6 PFU for the dams and 1.5 × 10^6 PFU for the infants of SARS-CoV-2 (2019-nCoV/USA-WA1/2020). The stock was obtained from BEI Resources (NR-52281). The stock underwent deep sequencing to confirm homology with the WA1/2020 isolate. Virus was stored at −80°C prior to use, thawed rapidly at 37°C, and placed immediately on wet ice. Nasal swabs, pharyngeal swabs, BAL, blood, breast milk and rectal swab samples were collected 1 week before infection and every 2–3 days post-challenge. Nasopharyngeal, oropharyngeal and buccal secretions were collected with FLOQSwabs™ (Copan), placed in a vial with DNA/RNA Shield™ solution (Zymo Research), and stored at −70°C until further processing.

BAL was performed using a 20F rubber feeding tube with instillation of 20 ml sterile physiologic saline followed by aspiration with a syringe. BAL samples were spun in the lab. The BAL cell pellet, together with 0.5 ml of supernatant, was then mixed with 1.5 ml of TRIzol®-LS (Thermo Fisher Scientific) and cryopreserved at −70° C. Additional aliquots of BAL supernatant were also immediately cryopreserved. Blood and milk were collected and processed as previously described (17–19).

Radiographs were obtained with a HF100+ Ultralight imaging unit (MinXRay, Northbrook, IL) at 50 kVp, 40mA, and 0.1 sec. Ventrodorsal, dorsoventral, R lateral, and L lateral radiographs were obtained prior to inoculation and on days 1, 3, 5, 7, 10, and 14 post inoculation. Radiographs were scored for the presence of pulmonary infiltrates by a board-certified veterinary radiologist, who was blinded to the experimental group and time point, according to a standard scoring system (0: normal; 1: mild interstitial pulmonary infiltrates; 2: moderate pulmonary infiltrates perhaps with partial cardiac border effacement and small areas of pulmonary consolidation; 3: severe interstitial infiltrates, large areas of pulmonary consolidation, alveolar patterns and air bronchograms). Individual lobes were scored and scores per animal per day were totaled.

At the end of the study, animals were euthanized, and a full necropsy was performed for tissue collection, including trachea for cell isolation and fixed lung tissues for histopathology.

Trachea collection and cell processing

Upon necropsy, tracheobronchial tissues were collected. Airway epithelial cells were isolated by placing tracheas in Minimum Essential Medium Eagle; Joklik Modification (Lonza) containing 0.1% type XIV protease (Sigma-Aldrich), 50 U/mL penicillin, 50 μg/mL each streptomycin and gentamicin, and 100 μg/mL geneticin G418 (Invitrogen) overnight. Cells were gently aspirated off and stored in liquid nitrogen prior to RNA isolation.

Viral load assay

SARS-CoV-2 infection was determined by quantitative Polymerase Chain Reaction (qPCR) of SARS-CoV-2 Genomic (orf1a) and Subgenomic (N) RNA.

SARS-CoV-2 Genomic (orf1a) qPCR.—A QIAsymphony SP (Qiagen, Hilden, Germany) automated sample preparation platform along with a virus/pathogen DSP midi kit and the complex800 protocol were used to extract viral RNA from 800 μL of respiratory sample. A reverse primer specific to the orf1a sequence of SARS-CoV-2 (5'-CGTGCCTACAGTACTCAGAATC-3') was annealed to the extracted RNA and then reverse transcribed into cDNA using SuperScript™ III Reverse Transcriptase (Thermo Fisher Scientific, Waltham, MA) along with RNAse Out (Thermo Fisher Scientific, Waltham, MA). The resulting cDNA was then treated with Rnase H (Thermo Fisher Scientific, Waltham, MA) and added to a custom 4x TaqMan™ Gene Expression Master Mix (Thermo Fisher Scientific, Waltham, MA) containing primers and a fluorescently labeled hydrolysis probe specific for the orf1a sequence of SARS-CoV-2 (forward primer 5'-GTGCTCATGGATGGCTCTATTA-3', reverse primer 5'-CGTGCCTACAGTACTCAGAATC-3', probe 5'-/56-FAM/ ACCTACCTT/ZEN/ GAAGGTTCTGTTAGAGTG GT/3IABkFQ/−3). All PCR setup steps were performed using QIAgility instruments (Qiagen, Hilden, Germany). The qPCR was then carried out on a QuantStudio 3 Real-Time PCR System (Thermo Fisher Scientific, Waltham, MA). SARS-CoV-2 genomic (orf1a) RNA copies per reaction were interpolated using quantification cycle data and a serial dilution of a highly characterized custom RNA transcript containing the SARS-CoV-2 orf1a sequence. Mean RNA copies per milliliter were then calculated by applying the assay dilution factor (DF=11.7). The limit of quantification (LOQ) for this assay is approximately 31 RNA cp/mL (1.49 log10) with 800 uL of sample.

Subgenomic (N) RNA qPCR assay.—A QIAsymphony SP (Qiagen, Hilden, Germany) automated sample preparation platform along with a virus/pathogen DSP midi kit and the complex800 protocol were used to extract viral RNA from 800 μL of respiratory sample. The extracted RNA was then added to TaqMan™ Fast Virus 1-Step Master Mix (Thermo Fisher Scientific, Waltham, MA) containing primers and a fluorescently labeled hydrolysis probe specific for mRNA from the nucleocapsid gene of SARS-CoV-2 (forward primer 5'-CGATCTCTTGTAGATCTGTTCTC-3', reverse primer 5'-GGTGAACCAAGACGCAGTAT-3', probe 5'-/56-FAM/TAACCAGAA/ZEN/

TGGAGAACGCAGT GGG/3IABkFQ/−3'). All PCR setup steps were performed using QIAgility instruments (Qiagen, Hilden, Germany). The qPCR was carried out on a QuantStudio 3 Real-Time PCR System (Thermo Fisher Scientific, Waltham, MA). SARS-CoV-2 subgenomic (N) RNA copies per reaction were interpolated using quantification cycle data and a serial dilution of a highly characterized custom RNA transcript containing the SARS-CoV-2 subgenomic nucleocapsid sequence. Mean RNA copies per milliliter were then calculated by applying the assay dilution factor (DF=5.625). The limit of quantification (LOQ) for this assay is approximately 31 RNA cp/mL (1.49 log10) with 800 uL of sample.

Spike-specific IgG ELISA

IgG binding to the stabilized SARS-CoV-2 S protein S-2P was measured in plasma using ELISA as previously described (20). Three hundred eighty-four–well plates were coated overnight with S protein (2 μg/ml) produced by the Protein Production Facility (PPF) at the Duke Human Vaccine Institute. Plates were then blocked with assay diluent (PBS containing 4% whey, 15% normal goat serum, and 0.5% Tween 20). Ten serial fourfold dilutions starting at 1:10 for plasma and undiluted for breast milk were added to the plates and incubated for 1 hour, followed by detection with a horseradish peroxidase (HRP)–conjugated mouse anti-monkey IgG (SouthernBiotech). The plates were developed by using an 2,2′-azinobis(3-ethylbenzthiazolinesulfonic acid peroxidase substrate system (Colonial Scientific), and absorbance was read at 450 nm with a SpectraMax microplate reader (Molecular Devices). Results were calculated as AUC and EC_{50} values. AUC values were calculated using the trapezoidal rule. EC_{50} values were calculated by fitting a four-parameter logistic function using nonlinear regression. Pooled NHP convalescent serum to SARS-CoV-2 (BEI Resources, NR-52401) was used in all IgG assays to ensure interassay reproducibility, but standard curves were not developed given the lack of an SARS-CoV-2 RM-specific IgG reagent of known concentration. IgA binding to S2P was measured following a similar ELISA protocol but using as detection Ab anti-rhesus IgA 10F12-biotin (NHP Reagent Resource catalog AB_2819304) followed by Streptadividin-HRP (Pierce, catalog 21126).

Binding antibody multiplex assay

SARS-CoV-2 antigens, including whole S (produced by PPF), S1 (Sino Biological, catalog no. 40591-V08H), S2 (Sino Biological, catalog no. 40590-V08B), RBD (Sino Biological, catalog no.40592-V08H), and NTD (Sino Biological, catalog no. 40591-V49H) were conjugated to Magplex beads (Bio-Rad, Hercules, CA). The conjugated beads were incubated on filter plates (Millipore,Stafford, VA) for 30 min before plasma samples were added. Plasma samples were diluted in assay diluent [1% dry milk, 5% goat serum, and 0.05% Tween 20 in PBS (pH 7.4.)] at a 1:1000-point dilution. Beads and diluted samples were incubated for 30 min with gentle, rotation, and IgG binding was detected using a PE-conjugated mouse anti-monkey IgG (SouthernBiotech, Birmingham, Alabama) at 2 μg/ml. Plates were washed and acquired on a Bio-Plex 200 instrument (Bio-Rad, Hercules, CA), and IgG binding was reported as mean fluorescence intensity (MFI). To assess assay background, the MFIs of wells without sample (blank wells) were used, and nonspecific binding of the samples to unconjugated blank beads, was evaluated.

Pseudovirus Ab neutralization assay

SARS-CoV-2 neutralization was assessed with S-pseudotyped viruses in 293 T/ACE2 cells as a function of reductions in luciferase (Luc) reporter activity. 293 T/ACE2 cells were provided by M. Farzan and H. Mu at Scripps Florida. Cells were maintained in Dulbecco's modified Eagle's medium containing 10% fetal bovine serum (FBS), 25 mM Hepes, gentamycin (50 μg/ml), and puromycin (3 μg/ml). An expression plasmid encoding codon-optimized full-length S of the Wuhan-1 strain (VRC7480) was provided by B.S.G. and K.S.C. at the Vaccine Research Center, NIH (USA). The D614G amino acid change was introduced into VRC7480 by site-directed mutagenesis using the QuikChange Lightning Site-Directed Mutagenesis Kit from Agilent Technologies (catalog no. 210518). The mutation was confirmed by full-length S gene sequencing. Pseudovirions were produced in HEK293 T/17 cells (American Type Culture Collection, catalog no. CRL-11268) by transfection using Fugene 6 (Promega, catalog no. E2692) and a combination of S plasmid, lentiviral backbone plasmid (pCMV ΔR8.2), and firefly Luc reporter gene plasmid (pHR' CMV Luc) (78) in a 1:17:17 ratio. Transfections were allowed to proceed for 16 to 20 hours at 37°C. Medium was removed, monolayers were rinsed with growth medium, and 15 ml of fresh growth medium was added. Pseudovirus-containing culture medium was collected after an additional 2 days of incubation and was clarified of cells by low-speed centrifugation and 0.45-μm filtration and stored in aliquots at −80°C. Median tissue culture infectious dose assays were performed on thawed aliquots to determine the infectious dose for neutralization assays.

For neutralization, a pretitrated dose of pseudovirus was incubated with eight serial fivefold dilutions of serum samples in duplicate in a total volume of 150 μl for 1 hour at 37°C in 96-well flat-bottom poly-L-lysine–coated culture plates (Corning Biocoat). HEK 293T cells expressing ACE2 receptors were suspended using TrypLE Select Enzyme solution (Thermo Fisher Scientific) and immediately added to all wells (10,000 cells in 100 μl of growth medium per well). One set of eight control wells received cells and virus (virus control), and another set of eight wells received cells only (background control). After 66 to 72 hours of incubation, medium was removed by gentle aspiration and 30 μl of Promega 1X lysis buffer was added to all wells. After a 10-min incubation at RT, 100 μl of Bright-Glo Luc reagent was added to all wells. After 1 to 2 min, 110 μl of the cell lysate was transferred to a black/white plate (PerkinElmer). Luminescence was measured using a PerkinElmer Life Sciences, Model Victor2 luminometer. Neutralization titers are the serum dilution at which relative light units (RLUs) were reduced by either 50% (ID_{50}) or 80% (ID_{80}) compared with virus control wells after subtraction of background RLUs. Serum samples were heat-inactivated for 30 min at 56°C before assay.

Flow cytometry

Whole blood samples were stained fresh and acquired the same day. Fluorescence was measured using a BD Biosciences FACSymphony™ with FACSDiva™ version 8.0.1 software. Compensation, gating, and analysis were performed using FlowJo (Version 10). Gating strategy for innate immune subsets in whole blood after gating on singlets was performed as previously described (21). Fluorochromes used included: CD3/CD20-APC-

Cy7, CD14-A700, CD8-BUV 805, CD66-APC, HLA-DR-BV786, CD16-BV 605, CD123-BV421, and CD11c-Pe-Cy7.

RNA isolation and transcript analysis

Tracheal cells (epithelial, immune and mesenchymal) were lysed in 350 ul of Trizol, and RNA was extracted by phenol:chloroform method, and collected over RNAeasy column (Qiagen, Germantown, MD). The RNA concentration and integrity was determined on the NanoDrop ND-1000 (Thermo Fisher Scientific). 1000ng RNA from each sample was used as a template for preparing Illumina compatible libraries using the TruSeq RNA Library Prep Kit v2 (Illumina). Library sizes were checked using D5000 high sensitivity tape on the TapesSation 2200 (Agilent), and pooled libraries concentration were determined by Qubit 3.0 Fluorometer (Thermo Fisher Scientific). A library input of 1.8 pM with 1% PhiX (Illumina) spike-in was sequenced using the NextSeq 500 instrument with the NextSeq500/550 High Output v2.5 Kit (Illumina) and generated paired-end 76bp reads. Samples from all four animals (two dams and two infants) were processed and analyzed together.

Analysis of the bulk RNA-seq data

RNA-seq data were processed using the TrimGalore toolkit (22) which employs Cutadapt (23) to trim low quality bases and Illumina sequencing adapters from the 3' end of the reads. Only reads that were 20 nt or longer after trimming were kept for further analysis. Reads were mapped to the Mmul 10.99 version of the Macaca mulatta genome and transcriptome (24) using the STAR RNA-seq alignment tool (25). Only reads that mapped to a single genomic location were kept for subsequent analysis. The great majority of remaining trimmed and mapped reads (99.2%) were more than 70 bp long and the median length was 76 bp. Gene counts were compiled using the HTSeq tool (26). Only genes that had at least 10 reads (raw counts) in any given library were used in subsequent analysis (27). Normalization and differential expression were carried out using the DESeq2 (28) Bioconductor (29) package with the R statistical programming environment (30). To normalize for sequencing depth and RNA composition across different library sizes, DESeq2 corrects internally for these factors using the median of ratios method [61]. The false discovery rate was calculated to control for multiple hypothesis testing. Gene set enrichment analysis was performed to identify gene ontology terms and pathways associated with altered gene expression for each of the comparisons performed. Heatmaps include only significantly up or downregulated genes where both infants or both dams are higher/lower than each other to exclude genes where one animal dominated the response, potentially skewing the results.

Histopathology

The lungs were harvested and each lobe separated. All lobes were cannulated with 18-gauge blunt needles. All lobes were slowly infused with neutral buffered formalin at 30 cm fluid pressure. Once fully inflated (approx. 30 mins) the main bronchus was tied off and the lungs were placed in individual jars of formalin and fixed for 72 hours. Then they were sliced from the hilus towards the periphery into slabs approximately 5mm thick. Each slab was placed into a cassette recording its position in the stack and with further division of the slab into

smaller pieces if required to fit into the cassette. Tissues were then held in 70% ethanol until processing and paraffin embedding followed by sectioning at 5 μm and generation of hematoxylin and eosin (H&E) and Masson trichrome stained slides. Slides from every other slab of the right and left caudal lobes were examined independently by 2 ACVP board certified pathologists in a blinded manner.

Immunohistochemistry (IHC)

Substance P (Thermo Fisher) and protein gene product 9.5 (Millipore Sigma) antibodies were applied to 5μm paraffin sections. The EnVision system (Agilent) was used as the detection system with AEC (Agilent) as a chromogen. Paraffin sections were treated in an antigen unmasking solution (Vector) at 100°C for 20 minutes before incubation with a primary antibody. The slides were counterstained with Gill's hematoxylin (StatLab). Primary antibodies were replaced by rabbit isotype control (Thermo Fisher) and run with each staining series as the negative controls.

Biocontainment and biosafety

All work described here was performed with approved standard operating procedures for SARS-CoV-2 in a biosafety level 3 (BSL-3) facility conforming to requirements recommended in the Microbiological and Biomedical Laboratories, by the U.S. Department of Health and Human Service, the U.S. Public Health Service, and the U.S. Center for Disease Control and Prevention (CDC), and the NIH.

RESULTS

Experimental design and SARS-CoV-2 infection of dam/infant pairs

To investigate age-dependent differences in pathogenesis of SARS-CoV-2, two dams and their 6-month-old infants were inoculated intranasally and intratracheally with SARS-CoV-2 (WA strain). Nasal and pharyngeal swabs, bronchoalveolar lavage (BAL), blood, breast milk and rectal swabs were collected over time up to day 14 post-challenge (Fig. 1A).

To compare viral replication kinetics between the adult dams and infant macaques after SARS-CoV-2 infection, we performed both genomic (Orf1a gene) and subgenomic (N gene) PCR on nasal (dams only), pharyngeal, buccal and rectal swabs. Nasal swabs were not collected from infants due to restricted size of infant nostrils. As shown in Fig. 1B, we did not detect significant differences in viral loads between adults and infants in pharyngeal or BAL supernatant or BAL pellet samples. Low levels of viral RNA were detected in one of the 2 infants in buccal and rectal swabs (Fig. 1B), while no viral RNA was detected in breast milk.

We evaluated clinical symptoms and radiographic changes overtime. Mild symptoms, including occasional sneezing were reported. The radiographs were scored for the presence of pulmonary infiltrates, according to a standard scoring system (0 to 3 per lobe). Individual lobes were scored and scores per animal per day were totaled. Only the adult macaques had scores on multiple (≥2) days and the highest scores observed (score of 5) were from one of the adult macaques (Supplemental Fig. 1). Overall in both age groups the lesions in the

lung were minimal and largely resolved consisting of occasional foci of mild inflammation on HE stained sections. Trichrome stained sections did not show an overt increase in fibrosis in either group (Supplemental Fig. 2). There was no significant evidence of interstitial pneumonia in any animal, only occasional focal increase in interstitial cellularity and in some areas an increase in alveolar macrophages (Supplemental Fig. 2), as previously reported (31).

Systemic innate cellular and cytokine responses in SARS-CoV-2-infected dam and infant rhesus macaques

We evaluated innate immune cell subsets in the peripheral blood and observed no major differences in proportion of cells between infant and dams after SARS-CoV-2 infection (Fig. 2A). Interestingly, however circulating neutrophils (lineage-, CD66+) were higher in adults and total HLA-DR+ (lineage-, CD66-) cells, comprising of monocytes and dendritic cell subsets, were higher in infants prior to inoculation with SARS-CoV-2 (Fig. 2A). For plasma cytokine responses, we observed greater than a 2-fold increase in IL-6 (all 4 animals) and IP10 (CXCL10) (2 dams, 1 infant) as reported previously (21), and the anti-inflammatory mediator IL-1RA (1 dam, 2 infants) within 1-day post SARS-CoV-2 infection (Fig. 2B). One infant demonstrated increased production of IL-17 and GM-CSF at several time points post-infection (Fig. 2B). Interestingly, IL-8 was upregulated greater than 7-fold in 3 of the 4 animals at day 14 post-infection. However, we did not identify any specific cytokine signature that distinguished dams from infants.

Kinetics of neutralizing antibody (nAb) development between dam and infant rhesus macaques infected with SARS-CoV-2

We next measured anti-spike (S) binding and nAbs in serum and breast milk samples. With the limitation that the small group sizes preclude statistical significance, we found that while dams had higher serum S-binding IgG antibody titers than infants (Fig. 3A), infants demonstrated faster kinetics of nAb development. Infants had higher nAb titers at day 7 post-infection, yet similar nAb titers at day 14 post-infection compared to dams (Fig. 3B). S-binding IgG, but not IgA, was detected in breast milk of infected dams at day 14 post-infection (Fig. 3C). NAbs in breast milk were detected in one dam at day 14 post-infection (Fig. 3D). A multiplexed antibody binding assay did not detect differences in receptor binding domain (RBD), S1, S2, full S and N-terminal domain (NTD)-specific antibodies between SARS-CoV-2-infected dam and infant macaques at day 14 (Fig. 3E).

Age-dependent differences in transcriptomic responses in the trachea reveal downregulated interferon stimulated genes and cilia injury signatures in adult macaques

The hierarchical and principal component analyses and heatmap (Supplemental Fig. 3A–C) of the differentially expressed genes (DEGs) of tracheal cells (epithelial, immune and mesenchymal) demonstrated altered transcriptomic expression of infant and dam rhesus macaques on day 14 after SARS-CoV-2 infection, where mothers and offspring clustered with each other. To identify gene ontology (GO) and hallmark gene sets associated with altered expression, gene set enrichment analysis (GSEA) was performed (1). The Hallmark pathway analysis revealed significantly decreased trachea cell genes associated with the *Interferon Alpha* and *Interferon Gamma* Hallmark pathways in adult compared to infant

macaques (Fig. 4A). Specifically, *IFI6*, *XAF1*, *DDX60*, *OAS2*, *HERC6*, *MX2*, *IFI44L*, *IFIT1, SAMD9L, PARP14 and IFIT12* are decreased in both adults compared to their infants (Fig. 4B).

Alternatively, in the GO pathway analysis we identified an overwhelming signature of decreased cilia structure and function in adult compare to infant tracheas (Fig. 5A,B). In fact, all GO pathways that were significantly enriched among downregulated genes (FWER adjusted P-value ≤ 0.05) were related to cilia structure and motility (Supplemental Table 1). Considering SARS-CoV-2 infection induces a de-differentiation of multiciliated cells (32), these results suggest a prolonged impairment of cilia functions in adult compared to infant rhesus macaques 14 days after SARS-CoV-2 infection.

Conducting airways of SARS-CoV-2 infected adult macaques show a profibrotic transcriptomic signature

In both the GO and Hallmark pathway analyses, there was significant enrichment among upregulated genes (FWER adjusted P-value ≤ 0.05) for pathways associated with wound repair and fibrosis in adult compared with infant macaques at day 14 post infection. Of the 39 GO pathways that are significantly enriched among upregulated genes in the adult macaques (Supplemental Table 1), the overwhelming majority were associated with extracellular matrix (ECM) organization and ECM metabolism. Similarly, the Hallmark pathway analysis revealed multiple pathways associated with wound repair and fibrosis in adult macaques including *Epithelial mesenchymal transition, Angiogenesis, Coagulation, Hypoxia, Apoptosis and TGF beta signaling*. Of the most DEGs of the upregulated pathways in adults compared to infants, all of them were associated with the ECM (Fig. 6A). Additionally, we stained trachea tissue for protein gene product 9.5 (PGP 9.5) (also known as ubiquitin C-terminal hydrolase-L1 [UCH-L1]) (Fig. 6C–F) and Substance P (Sub P) (**Fig. G-J**), proteins involved in wound healing (33, 34), and they were higher in infant compared to adult tracheas.

DISCUSSION

In this study, we evaluated age-dependent differences in SARS-CoV-2 pathogenesis by inoculating dam-infant rhesus macaque pairs with SARS-CoV-2. In line with previous studies in nonhuman primates (15, 16, 35–38), we demonstrate that both infant and dam rhesus macaques became productively infected and exhibited no to mild clinical symptoms. Lung radiograph scores showed mild pulmonary infiltrates in both dams and infants, however only in dams were pulmonary infiltrates observed for multiple days (≥2). Histologic examination of pulmonary infiltrates was extremely minimal and largely resolving when examined day 14 post-infection. This is consistent with previous experiments (21).

While viral loads in pharyngeal swabs and BAL samples did not differ between dam and infant macaques, differences in antibody response kinetics between the dams and infants were observed. For example, while there were higher anti-spike IgG binding antibody titers in adult macaques at day 10 and 14 post-infection, infants exhibited higher nAb titers at day 7. These data suggest faster kinetics of SARS-CoV-2 nAb responses in infant macaques. In pediatric cohorts infected with SARS-CoV-2, results have been variable and levels of

nAbs have been reported as lower, higher or not different compared to infected adults (39–43). However, age-dependent differences in nAb development have been observed for other pathogens. For example, in HIV-1 infected children, circulating broadly neutralizing antibodies (bnAbs) arise earlier in infection, and have higher potency and breadth compared to adults (44–49). Future work using this model should include measurement of T cell subsets in both blood and lymphoid tissue as well as determination of breadth against multiple SARS-CoV-2 variants.

Although there were not major differences in serum cytokines between adult and infant SARS-CoV-2 infected macaques, we observed increases in relevant pro-inflammatory cytokines. For example, IL-6 and IP10 (CXCL10) were increased in 3 of the 4 animals within 1-day post SARS-CoV-2, mirroring what was previously reported in rhesus macaques and other animal models of SARS-CoV-2 infection (37, 50, 51). Following SARS-CoV-2 infected macaques for greater than 14 days would be worthwhile in observing late-onset pro-inflammatory signatures in older and infant animals. Additionally, measuring cytokines in tissues would give additional insight into age-dependent local responses to infection.

An increase in interferon alpha and gamma transcriptomic signatures were observed in infant macaques compared to dams. There were multiple ISGs that were upregulated in both infants compared to their dams, nearly all of which were previously shown to be significantly upregulated after SARS-CoV-2 infection, including *IRF3, TLR3, DHX58, IFIH1,* and *DDX58* (12). Considering trachea RNA-seq data was collected at day 14 post-inoculation in our study, when viral loads were not detectable anymore, it is possible that levels of some ISGs are upregulated in infants at baseline compared to adults. Indeed, this has been demonstrated in multiple pediatric cohorts where ISGs (52) and cytokines and chemokine genes (53) were increased in SARS-CoV-2-uninfected children compared to adults and an antiviral type-I IFN gene signature was induced after SARS-CoV-2 infection in neonatal rhesus macaques (54). These data suggest the IFN response in children is pre-activated in epithelial cells of the upper airways and stronger in immune cell subsets compared to adults.

There was an overwhelming signature of decreased cilia structure and function-related genes in adult compared to infant macaques. It has been previously demonstrated that SARS-CoV-2 infection leads to dedifferentiation of multi-ciliated cells in vitro and in vivo (32). Additionally, other groups have observed delayed repair responses after pulmonary injury in adults compared to neonates. For example, hypoxia or LPS-induced lung injury resulted in less lung inflammation and apoptosis in neonatal compared to adult mice, which was dependent on increased NF-κβ activation (55–57). These data and our results support the hypothesis that the impacts of SARS-CoV-2 infection in the airways, including inflammation, apoptosis and barrier permeability (that implicates cilia structure and function), are lessened in neonates and young children compared to adults.

We observed that multiple genes and pathways associated with ECM composition and metabolism, coagulation, angiogenesis and hypoxia are increased in the trachea of dams compared to infants. These profibrotic transcriptomic signatures suggest greater activation of the cellular repair process in response to injury and apoptosis in the upper airway in

adults compared to infants. Indeed, the deposition of multiple components of the lung ECM including hyaluronan and fibrinogen (58–60) as well as profibrotic macrophage accumulation (60) has been associated with severe COVID-19 in adults. Alterations in ECM can be not only a consequence of lung fibrosis but also a driver of its progression (61) and acute respiratory distress syndrome in adults is more often associated with permanent alveolar simplification and fibrosis and higher morbidity and mortality outcomes compared to infants or children (62, 63). An increase in ECM and collagen genes in the adult macaques may be indicative of a dysregulation of injury repair.

Our study has limitations. Firstly, we only infected two dam-infant macaque pairs and more animal numbers are needed to determine statistical differences. Additionally, a mock-inoculated control group is necessary to decipher whether the differences observed are due to SARS-CoV-2 infection alone, the age-dependent maturation of tissues and the immune response, and/or experimental procedures. Finally, the time of euthanasia was not focused on evaluating acute inflammatory responses in tissues, as at 2 weeks, virus replication is mainly gone and tissue responses reflect repair in this animal model, and we evaluated trachea instead of lung responses. However, our study is valuable in that it agrees with currently published data in SARS-CoV-2-infected pediatric and adult cohorts and furthers our understanding of why younger populations are less susceptible to severe COVID-19 compared to adults. Additionally, this model will allow further delineation of molecular mechanisms of age-dependent SARS-CoV-2 pathogenesis and assess efficacy of medical countermeasures in dam-infant pairs.

Supplementary Material

Refer to Web version on PubMed Central for supplementary material.

Acknowledgments

The work was supported by a CNPRC Pilot Program award, the Office of Research Infrastructure Program, Office of The Director, National Institutes of Health under Award Number P51OD011107, the NIAID DAIDS Nonhuman Primate Core Virology Laboratory for AIDS Vaccine Research and Development Contract #HHSN272201800003C, and the Duke Precision Genomics Collaboratory COVID-19 Early Career Investigator Pilot Grant Award. Work with live SARS-CoV-2 was performed under BSL3 in the Duke Regional Biocontainment Laboratory (RBL), which received partial support for construction from the National Institutes of Health, National Institute of Allergy and Infectious Diseases (UC6-AI058607, G20-AI167200).

REFERENCES

1. Roser M RH 2021. Coronavirus Disease (COVID-19)
2. Wu Z, and McGoogan JM 2020. Characteristics of and Important Lessons From the Coronavirus Disease 2019 (COVID-19) Outbreak in China: Summary of a Report of 72 314 Cases From the Chinese Center for Disease Control and Prevention. Jama 323: 1239–1242. [PubMed: 32091533]
3. Zhu N, Zhang D, Wang W, Li X, Yang B, Song J, Zhao X, Huang B, Shi W, Lu R, Niu P, Zhan F, Ma X, Wang D, Xu W, Wu G, Gao GF, and Tan W 2020. A Novel Coronavirus from Patients with Pneumonia in China, 2019. N Engl J Med 382: 727–733. [PubMed: 31978945]
4. Holshue ML, DeBolt C, Lindquist S, Lofy KH, Wiesman J, Bruce H, Spitters C, Ericson K, Wilkerson S, Tural A, Diaz G, Cohn A, Fox L, Patel A, Gerber SI, Kim L, Tong S, Lu X, Lindstrom S, Pallansch MA, Weldon WC, Biggs HM, Uyeki TM, and Pillai SK 2020. First Case of 2019 Novel Coronavirus in the United States. N Engl J Med 382: 929–936. [PubMed: 32004427]

5. Denison MR 2004. Severe acute respiratory syndrome coronavirus pathogenesis, disease and vaccines: an update. Pediatr Infect Dis J 23: S207–214. [PubMed: 15577575]

6. Assiri A, McGeer A, Perl TM, Price CS, Al Rabeeah AA, Cummings DA, Alabdullatif ZN, Assad M, Almulhim A, Makhdoom H, Madani H, Alhakeem R, Al-Tawfiq JA, Cotten M, Watson SJ, Kellam P, Zumla AI, Memish ZA, and Team KM-CI 2013. Hospital outbreak of Middle East respiratory syndrome coronavirus. N Engl J Med 369: 407–416. [PubMed: 23782161]

7. Khuri-Bulos N, Payne DC, Lu X, Erdman D, Wang L, Faouri S, Shehabi A, Johnson M, Becker MM, Denison MR, Williams JV, and Halasa NB 2014. Middle East respiratory syndrome coronavirus not detected in children hospitalized with acute respiratory illness in Amman, Jordan, March 2010 to September 2012. Clin Microbiol Infect 20: 678–682. [PubMed: 24313317]

8. Donnelly CA, Ghani AC, Leung GM, Hedley AJ, Fraser C, Riley S, Abu-Raddad LJ, Ho LM, Thach TQ, Chau P, Chan KP, Lam TH, Tse LY, Tsang T, Liu SH, Kong JH, Lau EM, Ferguson NM, and Anderson RM 2003. Epidemiological determinants of spread of causal agent of severe acute respiratory syndrome in Hong Kong. Lancet 361: 1761–1766. [PubMed: 12781533]

9. Yang X, Yu Y, Xu J, Shu H, Xia J, Liu H, Wu Y, Zhang L, Yu Z, Fang M, Yu T, Wang Y, Pan S, Zou X, Yuan S, and Shang Y 2020. Clinical course and outcomes of critically ill patients with SARS-CoV-2 pneumonia in Wuhan, China: a single-centered, retrospective, observational study. Lancet Respir Med.

10. Sheikh A, McMenamin J, Taylor B, Robertson C, Public Health S, and the EIIC 2021. SARS-CoV-2 Delta VOC in Scotland: demographics, risk of hospital admission, and vaccine effectiveness. Lancet 397: 2461–2462. [PubMed: 34139198]

11. Chou J, Thomas PG, and Randolph AG 2022. Immunology of SARS-CoV-2 infection in children. Nature immunology 23: 177–185. [PubMed: 35105983]

12. Loske J, Rohmel J, Lukassen S, Stricker S, Magalhaes VG, Liebig J, Chua RL, Thurmann L, Messingschlager M, Seegebarth A, Timmermann B, Klages S, Ralser M, Sawitzki B, Sander LE, Corman VM, Conrad C, Laudi S, Binder M, Trump S, Eils R, Mall MA, and Lehmann I 2021. Pre-activated antiviral innate immunity in the upper airways controls early SARS-CoV-2 infection in children. Nat Biotechnol.

13. Neeland MR, Bannister S, Clifford V, Dohle K, Mulholland K, Sutton P, Curtis N, Steer AC, Burgner DP, Crawford NW, Tosif S, and Saffery R 2021. Innate cell profiles during the acute and convalescent phase of SARS-CoV-2 infection in children. Nat Commun 12: 1084. [PubMed: 33597531]

14. Sposito B, Broggi A, Pandolfi L, Crotta S, Clementi N, Ferrarese R, Sisti S, Criscuolo E, Spreafico R, Long JM, Ambrosi A, Liu E, Frangipane V, Saracino L, Bozzini S, Marongiu L, Facchini FA, Bottazzi A, Fossali T, Colombo R, Clementi M, Tagliabue E, Chou J, Pontiroli AE, Meloni F, Wack A, Mancini N, and Zanoni I 2021. The interferon landscape along the respiratory tract impacts the severity of COVID-19. Cell 184: 4953–4968 e4916. [PubMed: 34492226]

15. Chandrashekar A, Liu J, Martinot AJ, McMahan K, Mercado NB, Peter L, Tostanoski LH, Yu J, Maliga Z, Nekorchuk M, Busman-Sahay K, Terry M, Wrijil LM, Ducat S, Martinez DR, Atyeo C, Fischinger S, Burke JS, Slein MD, Pessaint L, Van Ry A, Greenhouse J, Taylor T, Blade K, Cook A, Finneyfrock B, Brown R, Teow E, Velasco J, Zahn R, Wegmann F, Abbink P, Bondzie EA, Dagotto G, Gebre MS, He X, Jacob-Dolan C, Kordana N, Li Z, Lifton MA, Mahrokhian SH, Maxfield LF, Nityanandam R, Nkolola JP, Schmidt AG, Miller AD, Baric RS, Alter G, Sorger PK, Estes JD, Andersen H, Lewis MG, and Barouch DH 2020. SARS-CoV-2 infection protects against rechallenge in rhesus macaques. Science.

16. Williamson BN, Feldmann F, Schwarz B, Meade-White K, Porter DP, Schulz J, van Doremalen N, Leighton I, Yinda CK, Perez-Perez L, Okumura A, Lovaglio J, Hanley PW, Saturday G, Bosio CM, Anzick S, Barbian K, Cihlar T, Martens C, Scott DP, Munster VJ, and de Wit E 2020. Clinical benefit of remdesivir in rhesus macaques infected with SARS-CoV-2. Nature.

17. Permar SR, Wilks AB, Ehlinger EP, Kang HH, Mahlokozera T, Coffey RT, Carville A, Letvin NL, and Seaman MS 2010. Limited contribution of mucosal IgA to Simian immunodeficiency virus (SIV)-specific neutralizing antibody response and virus envelope evolution in breast milk of SIV-infected, lactating rhesus monkeys. Journal of virology 84: 8209–8218. [PubMed: 20519381]

18. Jensen K, Nabi R, Van Rompay KKA, Robichaux S, Lifson JD, Piatak M Jr., Jacobs WR Jr., Fennelly G, Canfield D, Mollan KR, Hudgens MG, Larsen MH, Amedee AM, Kozlowski PA, and

De Paris K 2016. Vaccine-Elicited Mucosal and Systemic Antibody Responses Are Associated with Reduced Simian Immunodeficiency Viremia in Infant Rhesus Macaques. Journal of virology 90: 7285–7302. [PubMed: 27252535]

19. Marthas ML, Van Rompay KK, Abbott Z, Earl P, Buonocore-Buzzelli L, Moss B, Rose NF, Rose JK, Kozlowski PA, and Abel K 2011. Partial efficacy of a VSV-SIV/MVA-SIV vaccine regimen against oral SIV challenge in infant macaques. Vaccine 29: 3124–3137. [PubMed: 21377510]
20. Dennis M, Eudailey J, Pollara J, McMillan AS, Cronin KD, Saha PT, Curtis AD, Hudgens MG, Fouda GG, Ferrari G, Alam M, Van Rompay KKA, De Paris K, Permar S, and Shen X 2019. Coadministration of CH31 Broadly Neutralizing Antibody Does Not Affect Development of Vaccine-Induced Anti-HIV-1 Envelope Antibody Responses in Infant Rhesus Macaques. Journal of virology 93.
21. Shaan Lakshmanappa Y, Elizaldi SR, Roh JW, Schmidt BA, Carroll TD, Weaver KD, Smith JC, Verma A, Deere JD, Dutra J, Stone M, Franz S, Sammak RL, Olstad KJ, Rachel Reader J, Ma ZM, Nguyen NK, Watanabe J, Usachenko J, Immareddy R, Yee JL, Weiskopf D, Sette A, Hartigan-O'Connor D, McSorley SJ, Morrison JH, Tran NK, Simmons G, Busch MP, Kozlowski PA, Van Rompay KKA, Miller CJ, and Iyer SS 2021. SARS-CoV-2 induces robust germinal center CD4 T follicular helper cell responses in rhesus macaques. Nat Commun 12: 541. [PubMed: 33483492]
22. Institute B Trim Galore.
23. Kechin A, Boyarskikh U, Kel A, and Filipenko M 2017. cutPrimers: A New Tool for Accurate Cutting of Primers from Reads of Targeted Next Generation Sequencing. Journal of computational biology : a journal of computational molecular cell biology 24: 1138–1143. [PubMed: 28715235]
24. Kersey PJ, Staines DM, Lawson D, Kulesha E, Derwent P, Humphrey JC, Hughes DS, Keenan S, Kerhornou A, Koscielny G, Langridge N, McDowall MD, Megy K, Maheswari U, Nuhn M, Paulini M, Pedro H, Toneva I, Wilson D, Yates A, and Birney E 2012. Ensembl Genomes: an integrative resource for genome-scale data from non-vertebrate species. Nucleic acids research 40: D91–97. [PubMed: 22067447]
25. Dobin A, Davis CA, Schlesinger F, Drenkow J, Zaleski C, Jha S, Batut P, Chaisson M, and Gingeras TR 2013. STAR: ultrafast universal RNA-seq aligner. Bioinformatics (Oxford, England) 29: 15–21. [PubMed: 23104886]
26. G Putri SA, PT Pyl JE Pimanda F Zanini. 2022. Analysing high-throughput sequencing data in Python with HTSeq 2.0.
27. Bourgon R, Gentleman R, and Huber W 2010. Independent filtering increases detection power for high-throughput experiments. Proc Natl Acad Sci U S A 107: 9546–9551. [PubMed: 20460310]
28. Love MI, Huber W, and Anders S 2014. Moderated estimation of fold change and dispersion for RNA-seq data with DESeq2. Genome biology 15: 550. [PubMed: 25516281]
29. Huber W, Carey VJ, Gentleman R, Anders S, Carlson M, Carvalho BS, Bravo HC, Davis S, Gatto L, Girke T, Gottardo R, Hahne F, Hansen KD, Irizarry RA, Lawrence M, Love MI, MacDonald J, Obenchain V, Oleś AK, Pagès H, Reyes A, Shannon P, Smyth GK, Tenenbaum D, Waldron L, and Morgan M 2015. Orchestrating high-throughput genomic analysis with Bioconductor. Nature methods 12: 115–121. [PubMed: 25633503]
30. The R Project for Statistical Computing.
31. Van Rompay KKA, Olstad KJ, Sammak RL, Dutra J, Watanabe JK, Usachenko JL, Immareddy R, Verma A, Shaan Lakshmanappa Y, Schmidt BA, Roh JW, Elizaldi SR, Allen AM, Muecksch F, Lorenzi JCC, Lockwood S, Pollard RE, Yee JL, Nham PB, Ardeshir A, Deere JD, Patterson J, Dang Q, Hatziioannou T, Bieniasz PD, Iyer SS, Hartigan-O'Connor DJ, Nussenzweig MC, and Reader JR 2021. Early treatment with a combination of two potent neutralizing antibodies improves clinical outcomes and reduces virus replication and lung inflammation in SARS-CoV-2 infected macaques. PLoS pathogens 17: e1009688. [PubMed: 34228761]
32. Robinot R, Hubert M, de Melo GD, Lazarini F, Bruel T, Smith N, Levallois S, Larrous F, Fernandes J, Gellenoncourt S, Rigaud S, Gorgette O, Thouvenot C, Trébeau C, Mallet A, Duménil G, Gobaa S, Etournay R, Lledo PM, Lecuit M, Bourhy H, Duffy D, Michel V, Schwartz O, and Chakrabarti LA 2021. SARS-CoV-2 infection induces the dedifferentiation of multiciliated cells and impairs mucociliary clearance. Nat Commun 12: 4354. [PubMed: 34272374]

33. Leal EC, Carvalho E, Tellechea A, Kafanas A, Tecilazich F, Kearney C, Kuchibhotla S, Auster ME, Kokkotou E, Mooney DJ, LoGerfo FW, Pradhan-Nabzdyk L, and Veves A 2015. Substance P promotes wound healing in diabetes by modulating inflammation and macrophage phenotype. The American journal of pathology 185: 1638–1648. [PubMed: 25871534]
34. Liu H, Povysheva N, Rose ME, Mi Z, Banton JS, Li W, Chen F, Reay DP, Barrionuevo G, Zhang F, and Graham SH 2019. Role of UCHL1 in axonal injury and functional recovery after cerebral ischemia. 116: 4643–4650.
35. Speranza E, Purushotham JN, Port JR, Schwarz B, Flagg M, Williamson BN, Feldmann F, Singh M, Pérez-Pérez L, Sturdevant GL, Roberts LM, Carmody A, Schulz JE, van Doremalen N, Okumura A, Lovaglio J, Hanley PW, Shaia C, Germain RN, Best SM, Munster VJ, Bosio CM, and de Wit E 2022. Age-related differences in immune dynamics during SARS-CoV-2 infection in rhesus macaques. Life science alliance 5.
36. Singh DK, Singh B, Ganatra SR, Gazi M, Cole J, Thippeshappa R, Alfson KJ, Clemmons E, Gonzalez O, Escobedo R, Lee TH, Chatterjee A, Goez-Gazi Y, Sharan R, Gough M, Alvarez C, Blakley A, Ferdin J, Bartley C, Staples H, Parodi L, Callery J, Mannino A, Klaffke B, Escareno P, Platt RN 2nd, Hodara V, Scordo J, Gautam S, Vilanova AG, Olmo-Fontanez A, Schami A, Oyejide A, Ajithdoss DK, Copin R, Baum A, Kyratsous C, Alvarez X, Ahmed M, Rosa B, Goodroe A, Dutton J, Hall-Ursone S, Frost PA, Voges AK, Ross CN, Sayers K, Chen C, Hallam C, Khader SA, Mitreva M, Anderson TJC, Martinez-Sobrido L, Patterson JL, Turner J, Torrelles JB, Dick EJ Jr., Brasky K, Schlesinger LS, Giavedoni LD, Carrion R Jr., and Kaushal D 2021. Responses to acute infection with SARS-CoV-2 in the lungs of rhesus macaques, baboons and marmosets. Nature microbiology 6: 73–86.
37. Munster VJ, Feldmann F, Williamson BN, van Doremalen N, Pérez-Pérez L, Schulz J, Meade-White K, Okumura A, Callison J, Brumbaugh B, Avanzato VA, Rosenke R, Hanley PW, Saturday G, Scott D, Fischer ER, and de Wit E 2020. Respiratory disease in rhesus macaques inoculated with SARS-CoV-2. Nature 585: 268–272. [PubMed: 32396922]
38. Rockx B, Kuiken T, Herfst S, Bestebroer T, Lamers MM, Oude Munnink BB, de Meulder D, van Amerongen G, van den Brand J, Okba NMA, Schipper D, van Run P, Leijten L, Sikkema R, Verschoor E, Verstrepen B, Bogers W, Langermans J, Drosten C, Fentener van Vlissingen M, Fouchier R, de Swart R, Koopmans M, and Haagmans BL 2020. Comparative pathogenesis of COVID-19, MERS, and SARS in a nonhuman primate model. Science 368: 1012–1015. [PubMed: 32303590]
39. Weisberg SP, Connors TJ, Zhu Y, Baldwin MR, Lin WH, Wontakal S, Szabo PA, Wells SB, Dogra P, Gray J, Idzikowski E, Stelitano D, Bovier FT, Davis-Porada J, Matsumoto R, Poon MML, Chait M, Mathieu C, Horvat B, Decimo D, Hudson KE, Zotti FD, Bitan ZC, La Carpia F, Ferrara SA, Mace E, Milner J, Moscona A, Hod E, Porotto M, and Farber DL 2021. Distinct antibody responses to SARS-CoV-2 in children and adults across the COVID-19 clinical spectrum. Nature immunology 22: 25–31. [PubMed: 33154590]
40. Garrido C, Hurst JH, Lorang CG, Aquino JN, Rodriguez J, Pfeiffer TS, Singh T, Semmes EC, Lugo DJ, Rotta AT, Turner NA, Burke TW, McClain MT, Petzold EA, Permar SR, Moody MA, Woods CW, Kelly MS, and Fouda GG 2021. Asymptomatic or mild symptomatic SARS-CoV-2 infection elicits durable neutralizing antibody responses in children and adolescents. JCI insight 6.
41. Yang HS, Costa V, Racine-Brzostek SE, Acker KP, Yee J, Chen Z, Karbaschi M, Zuk R, Rand S, Sukhu A, Klasse PJ, Cushing MM, Chadburn A, and Zhao Z 2021. Association of Age With SARS-CoV-2 Antibody Response. JAMA network open 4: e214302. [PubMed: 33749770]
42. Pierce CA, Preston-Hurlburt P, Dai Y, Aschner CB, Cheshenko N, Galen B, Garforth SJ, Herrera NG, Jangra RK, Morano NC, Orner E, Sy S, Chandran K, Dziura J, Almo SC, Ring A, Keller MJ, Herold KC, and Herold BC 2020. Immune responses to SARS-CoV-2 infection in hospitalized pediatric and adult patients. Sci Transl Med 12: eabd5487. [PubMed: 32958614]
43. Dowell AC, Butler MS, Jinks E, Tut G, Lancaster T, Sylla P, Begum J, Bruton R, Pearce H, Verma K, Logan N, Tyson G, Spalkova E, Margielewska-Davies S, Taylor GS, Syrimi E, Baawuah F, Beckmann J, Okike IO, Ahmad S, Garstang J, Brent AJ, Brent B, Ireland G, Aiano F, Amin-Chowdhury Z, Jones S, Borrow R, Linley E, Wright J, Azad R, Waiblinger D, Davis C, Thomson EC, Palmarini M, Willett BJ, Barclay WS, Poh J, Amirthalingam G, Brown KE, Ramsay ME, Zuo J, Moss P, and Ladhani S 2022. Children develop robust and sustained cross-reactive spike-

specific immune responses to SARS-CoV-2 infection. Nature immunology 23: 40–49. [PubMed: 34937928]

44. Muenchhoff M, Adland E, Karimanzira O, Crowther C, Pace M, Csala A, Leitman E, Moonsamy A, McGregor C, Hurst J, Groll A, Mori M, Sinmyee S, Thobakgale C, Tudor-Williams G, Prendergast AJ, Kloverpris H, Roider J, Leslie A, Shingadia D, Brits T, Daniels S, Frater J, Willberg CB, Walker BD, Ndung'u T, Jooste P, Moore PL, Morris L, and Goulder P 2016. Nonprogressing HIV-infected children share fundamental immunological features of nonpathogenic SIV infection. Sci Transl Med 8: 358ra125.
45. Ditse Z, Muenchhoff M, Adland E, Jooste P, Goulder P, Moore PL, and Morris L 2018. HIV-1 Subtype C-Infected Children with Exceptional Neutralization Breadth Exhibit Polyclonal Responses Targeting Known Epitopes. Journal of virology 92.
46. Goo L, Chohan V, Nduati R, and Overbaugh J 2014. Early development of broadly neutralizing antibodies in HIV-1-infected infants. Nature medicine 20: 655–658.
47. Makhdoomi MA, Khan L, Kumar S, Aggarwal H, Singh R, Lodha R, Singla M, Das BK, Kabra SK, and Luthra K 2017. Evolution of cross-neutralizing antibodies and mapping epitope specificity in plasma of chronic HIV-1-infected antiretroviral therapy-naïve children from India. The Journal of general virology 98: 1879–1891. [PubMed: 28696188]
48. Mishra N, Sharma S, Dobhal A, Kumar S, Chawla H, Singh R, Makhdoomi MA, Das BK, Lodha R, Kabra SK, and Luthra K 2020. Broadly neutralizing plasma antibodies effective against autologous circulating viruses in infants with multivariant HIV-1 infection. Nat Commun 11: 4409. [PubMed: 32879304]
49. Kumar S, Panda H, Makhdoomi MA, Mishra N, Safdari HA, Chawla H, Aggarwal H, Reddy ES, Lodha R, Kumar Kabra S, Chandele A, Dutta S, and Luthra K 2019. An HIV-1 Broadly Neutralizing Antibody from a Clade C-Infected Pediatric Elite Neutralizer Potently Neutralizes the Contemporaneous and Autologous Evolving Viruses. Journal of virology 93.
50. Francis ME, Goncin U, Kroeker A, Swan C, Ralph R, Lu Y, Etzioni AL, Falzarano D, Gerdts V, Machtaler S, Kindrachuk J, and Kelvin AA 2021. SARS-CoV-2 infection in the Syrian hamster model causes inflammation as well as type I interferon dysregulation in both respiratory and non-respiratory tissues including the heart and kidney. PLoS pathogens 17: e1009705. [PubMed: 34265022]
51. Winkler ES, Bailey AL, Kafai NM, Nair S, McCune BT, Yu J, Fox JM, Chen RE, Earnest JT, Keeler SP, Ritter JH, Kang LI, Dort S, Robichaud A, Head R, Holtzman MJ, and Diamond MS 2020. SARS-CoV-2 infection of human ACE2-transgenic mice causes severe lung inflammation and impaired function. Nature immunology 21: 1327–1335. [PubMed: 32839612]
52. Yoshida M, Worlock KB, Huang N, Lindeboom RGH, Butler CR, Kumasaka N, Conde CD, Mamanova L, Bolt L, Richardson L, Polanski K, Madissoon E, Barnes JL, Allen-Hyttinen J, Kilich E, Jones BC, de Wilton A, Wilbrey-Clark A, Sungnak W, Pett JP, Weller J, Prigmore E, Yung H, Mehta P, Saleh A, Saigal A, Chu V, Cohen JM, Cane C, Iordanidou A, Shibuya S, Reuschl AK, Herczeg IT, Argento AC, Wunderink RG, Smith SB, Poor TA, Gao CA, Dematte JE, Reynolds G, Haniffa M, Bowyer GS, Coates M, Clatworthy MR, Calero-Nieto FJ, Göttgens B, O'Callaghan C, Sebire NJ, Jolly C, de Coppi P, Smith CM, Misharin AV, Janes SM, Teichmann SA, Nikolić MZ, and Meyer KB 2021. Local and systemic responses to SARS-CoV-2 infection in children and adults. Nature.
53. Loske J, Röhmel J, Lukassen S, Stricker S, Magalhães VG, Liebig J, Chua RL, Thürmann L, Messingschlager M, Seegebarth A, Timmermann B, Klages S, Ralser M, Sawitzki B, Sander LE, Corman VM, Conrad C, Laudi S, Binder M, Trump S, Eils R, Mall MA, and Lehmann I 2021. Pre-activated antiviral innate immunity in the upper airways controls early SARS-CoV-2 infection in children. Nature Biotechnology.
54. Fovet CM, Pimienta C, Galhaut M, Relouzat F, Nunez N, Cavarelli M, Sconosciuti Q, Dhooge N, Marzinotto I, Lampasona V, Tolazzi M, Scarlatti G, Ho Tsong Fang R, Naninck T, Dereuddre-Bosquet N, Van Wassenhove J, Gallouët AS, Maisonnasse P, Le Grand R, Menu E, and Seddiki N 2022. A Case Study to Dissect Immunity to SARS-CoV-2 in a Neonate Nonhuman Primate Model. Frontiers in immunology 13: 855230. [PubMed: 35603150]

55. Alvira CM, Abate A, Yang G, Dennery PA, and Rabinovitch M 2007. Nuclear factor-kappaB activation in neonatal mouse lung protects against lipopolysaccharide-induced inflammation. American journal of respiratory and critical care medicine 175: 805–815. [PubMed: 17255561]
56. Yang G, Abate A, George AG, Weng YH, and Dennery PA 2004. Maturational differences in lung NF-kappaB activation and their role in tolerance to hyperoxia. The Journal of clinical investigation 114: 669–678. [PubMed: 15343385]
57. Ying L, Alvira CM, and Cornfield DN 2018. Developmental differences in focal adhesion kinase expression modulate pulmonary endothelial barrier function in response to inflammation. American journal of physiology. Lung cellular and molecular physiology 315: L66–l77. [PubMed: 29597831]
58. Hellman U, Karlsson MG, Engström-Laurent A, Cajander S, Dorofte L, Ahlm C, Laurent C, and Blomberg A 2020. Presence of hyaluronan in lung alveoli in severe Covid-19: An opening for new treatment options? The Journal of biological chemistry 295: 15418–15422. [PubMed: 32978255]
59. Wool GD, and Miller JL 2021. The Impact of COVID-19 Disease on Platelets and Coagulation. Pathobiology : journal of immunopathology, molecular and cellular biology 88: 15–27. [PubMed: 33049751]
60. Wendisch D, Dietrich O, Mari T, von Stillfried S, Ibarra IL, Mittermaier M, Mache C, Chua RL, Knoll R, Timm S, Brumhard S, Krammer T, Zauber H, Hiller AL, Pascual-Reguant A, Mothes R, Bülow RD, Schulze J, Leipold AM, Djudjaj S, Erhard F, Geffers R, Pott F, Kazmierski J, Radke J, Pergantis P, Baßler K, Conrad C, Aschenbrenner AC, Sawitzki B, Landthaler M, Wyler E, Horst D, Hippenstiel S, Hocke A, Heppner FL, Uhrig A, Garcia C, Machleidt F, Herold S, Elezkurtaj S, Thibeault C, Witzenrath M, Cochain C, Suttorp N, Drosten C, Goffinet C, Kurth F, Schultze JL, Radbruch H, Ochs M, Eils R, Müller-Redetzky H, Hauser AE, Luecken MD, Theis FJ, Conrad C, Wolff T, Boor P, Selbach M, Saliba AE, and Sander LE 2021. SARS-CoV-2 infection triggers profibrotic macrophage responses and lung fibrosis. Cell 184: 6243–6261.e6227. [PubMed: 34914922]
61. Herrera J, Henke CA, and Bitterman PB 2018. Extracellular matrix as a driver of progressive fibrosis. The Journal of clinical investigation 128: 45–53. [PubMed: 29293088]
62. Im D, Shi W, and Driscoll B 2016. Pediatric Acute Respiratory Distress Syndrome: Fibrosis versus Repair. Front Pediatr 4: 28–28. [PubMed: 27066462]
63. Orloff KE, Turner DA, and Rehder KJ 2019. The Current State of Pediatric Acute Respiratory Distress Syndrome. Pediatric allergy, immunology, and pulmonology 32: 35–44. [PubMed: 31236307]

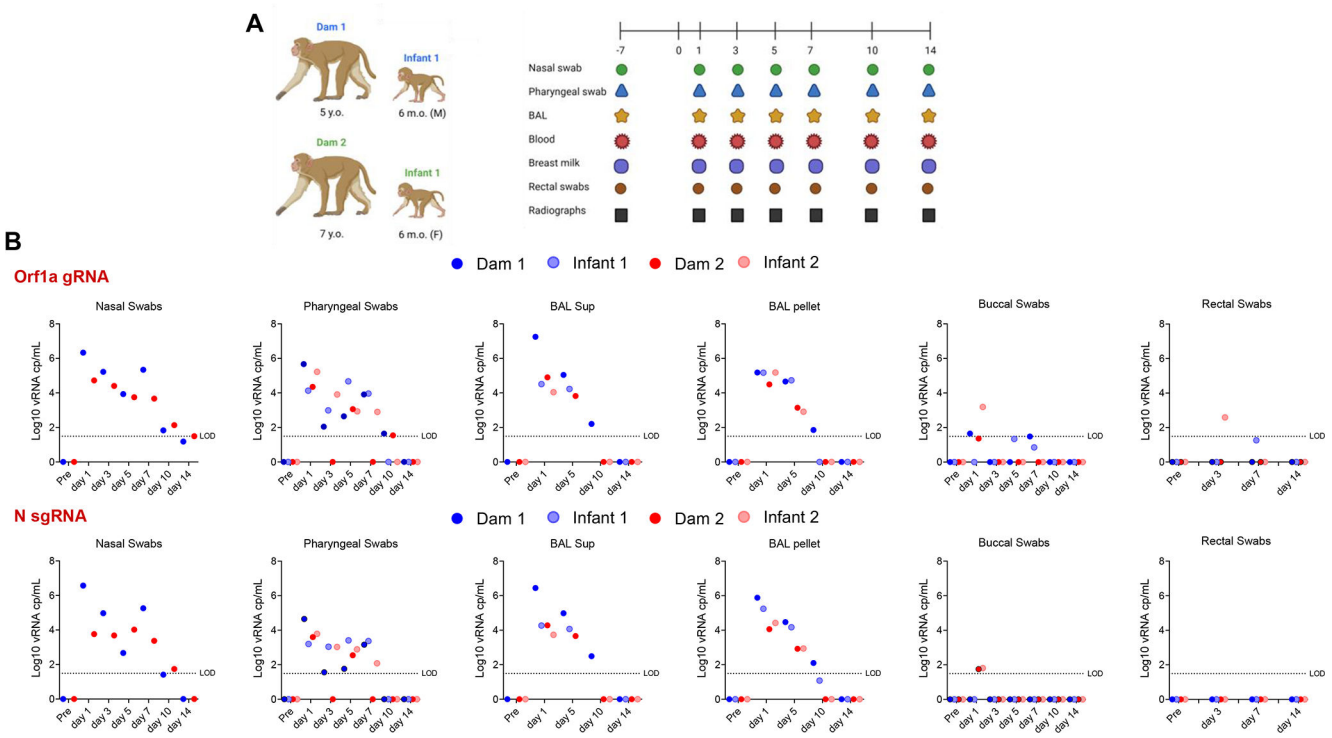

FIG 1.

Experimental design and SARS-CoV-2 RNA shedding. (A) Two dams and their respectively 6-month-old infants were inoculated intratracheally and intranasally with 2.5×10^6 PFU and 1.5×10^6 PFU of SARS-CoV-2 (WA strain), respectively. Nasal and pharyngeal swabs, bronchoalveolar lavage (BAL), blood, breast milk and rectal swabs were collected over time up to day 14 post-challenge. Additionally, lung radiographs were performed throughout the experiment. (B) Log_{10} viral RNA copies per mL are reported for nasal swabs, pharyngeal swabs, BAL supernatants and pellets, buccal swabs and rectal swabs over time for both the genomic (Orf1a gene) and subgenomic (N gene) viral RNA.

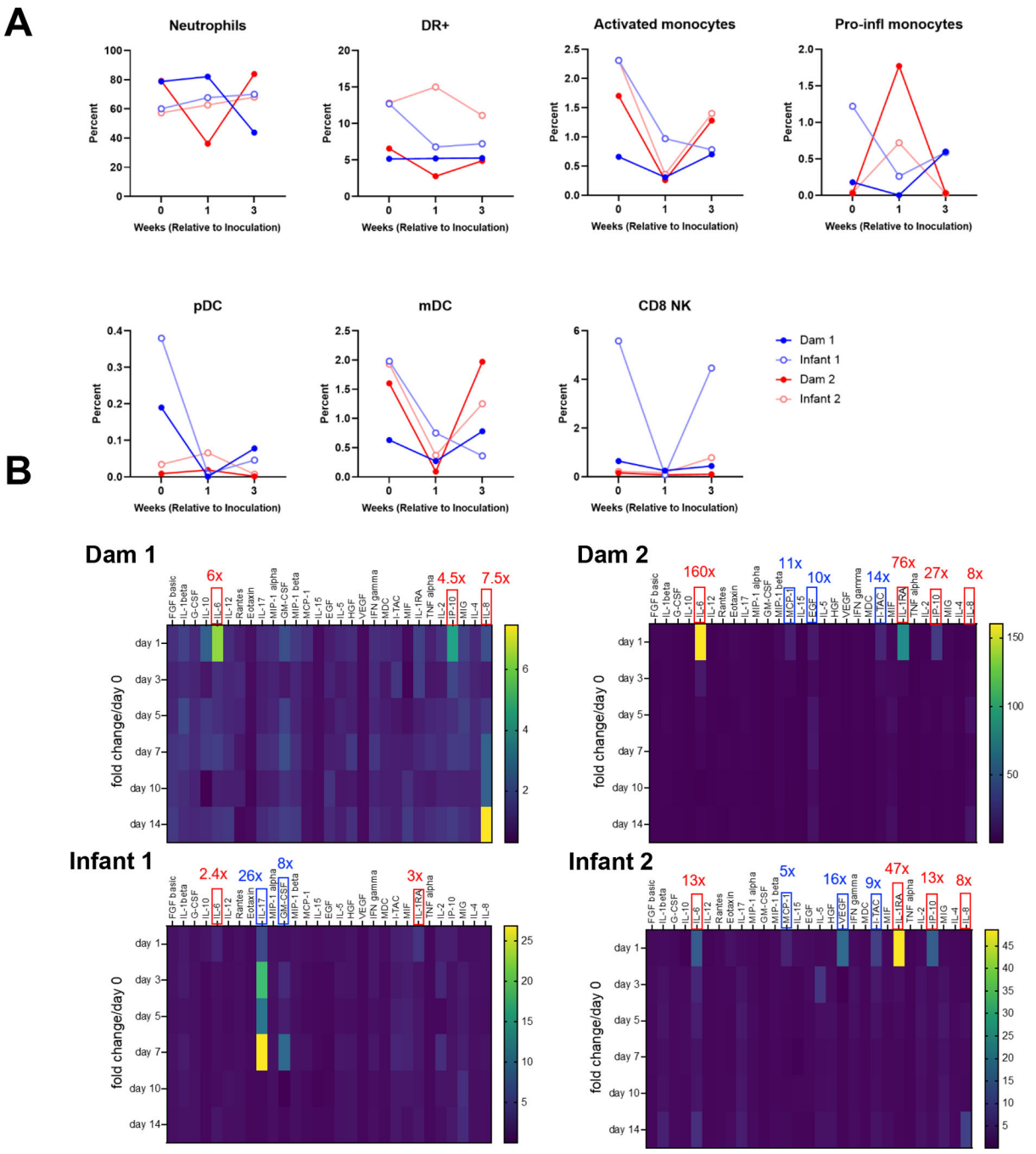

FIG 2.

Circulating innate immune cell and cytokine responses in SARS-CoV-2-infected dam and infant rhesus macaques (A) Kinetics of innate immune cell responses including neutrophils, total HLA-DR+ (lineage-, CD66-) cells, activated monocytes, pro-inflammatory monocytes, plasmacytoid dendritic cells (pDC), myeloid dendritic cells (mDC) and $CD8^{+}$ natural killer (NK) cells. (B) Heat maps of innate cytokines for each animal represented as fold change over day 0 post SARS-CoV-2 infection. Notable increases in key cytokines observed in all animals are denoted in red box, while increase in key cytokines observed in individual

animals are denoted in blue box (values represent peak fold change over day 0). The scale to the right of the heat map is in pg/ml.

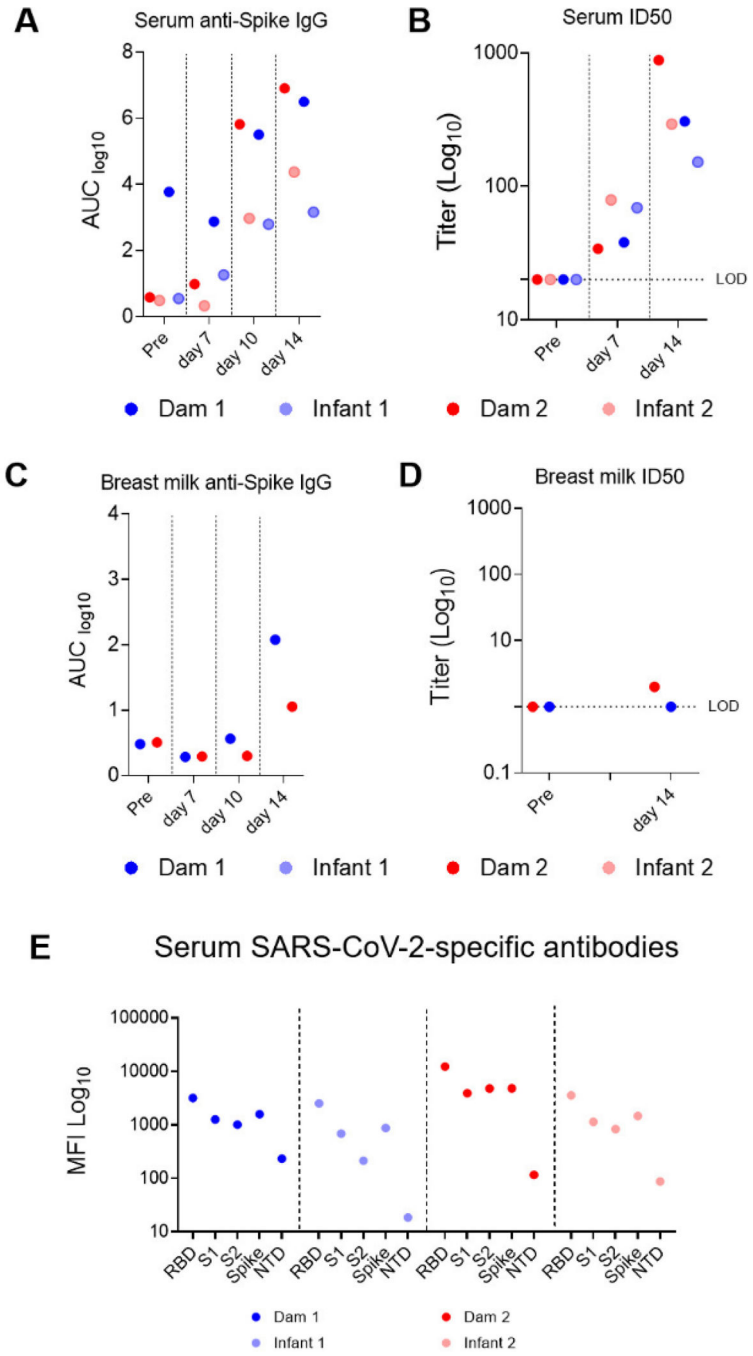

FIG 3.

SARS-CoV-2-elicited binding and neutralizing antibody (nAb) responses in infant and dam rhesus macaques (A) S-2P protein-specific antibody responses were measured in serum and (C) breast milk by ELISA. Serial dilutions of plasma (starting at 1:10) and breast milk (starting at 1:1) were assayed for IgG binding to SARS-CoV-2 S. Data are reported as $\log_{10}$ AUC values. (B) Neutralization capacity in serum and (D) breast milk was measured using S D614G-pseudotyped viruses and HEK 293T cells expressing ACE2 receptors. Results are expressed as reciprocal 50% inhibitory dilution (ID_{50}). Gray dotted lines represent

detection cutoff. (E) Antibody epitope specificity measured by binding antibody multiplex assay (BAMA). Plasma was diluted 1:10,000 to measure binding to different domains of the S protein, including the RBD, S1, S2, full-length S protein, and NTD. Binding antibody responses are reported as $\log_{10}$-transformed MFI after subtraction of background values.

A

PATHWAY NAME	SIZE	ES	NES	NOM p-val	FDR q-val	FWER p-val
HALLMARK_INTERFERON_ALPHA_RESPONSE	82	-0.53617	-2.09733	0	0	0
HALLMARK_INTERFERON_GAMMA_RESPONSE	176	-0.45318	-1.96484	0	2.24E-04	0.001

B

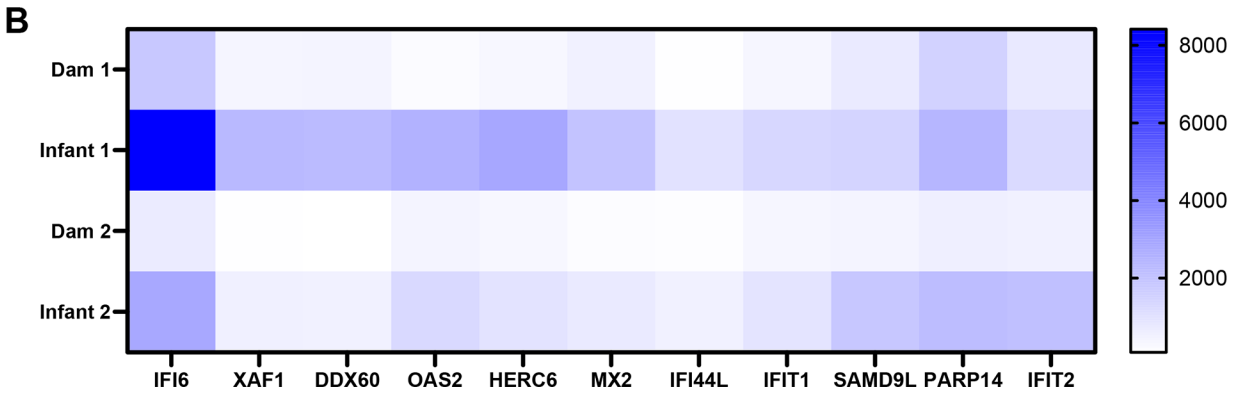

FIG 4.

Age-dependent differences in transcriptomic responses in the trachea reveal downregulated interferon (IFN) stimulated genes in adult macaques. (A) Hallmark pathways significantly (p-value ≤0.05) enriched among downregulated genes in adult compared with infant macaques 14 days after SARS-CoV-2 infection. (B) Heat map of differentially expressed IFN stimulated genes from *Interferon Alpha Response* and *Interferon Gamma Response* Hallmark pathways (p-value ≤0.05). Blue represents relative upregulation of gene expression and white represents relative downregulation of gene expression. Genes are arranged by $\log_2$ fold change with the largest $\log_2$ fold change to the left and the smallest $\log_2$ fold change to the right.

A

PATHWAY NAME	SIZE	ES	NES	NOM p-val	FDR q-val	FWER p-val
GO_CILIUM_ORGANIZATION	146	-0.65847	-2.78106	0	0	0
GO_CILIUM_MORPHOGENESIS	161	-0.6283	-2.69571	0	0	0
GO_AXONEME_ASSEMBLY	30	-0.85359	-2.69118	0	0	0
GO_CILIARY_PLASM	64	-0.71121	-2.61748	0	0	0
GO_CILIUM_MOVEMENT	28	-0.81316	-2.56238	0	0	0

B

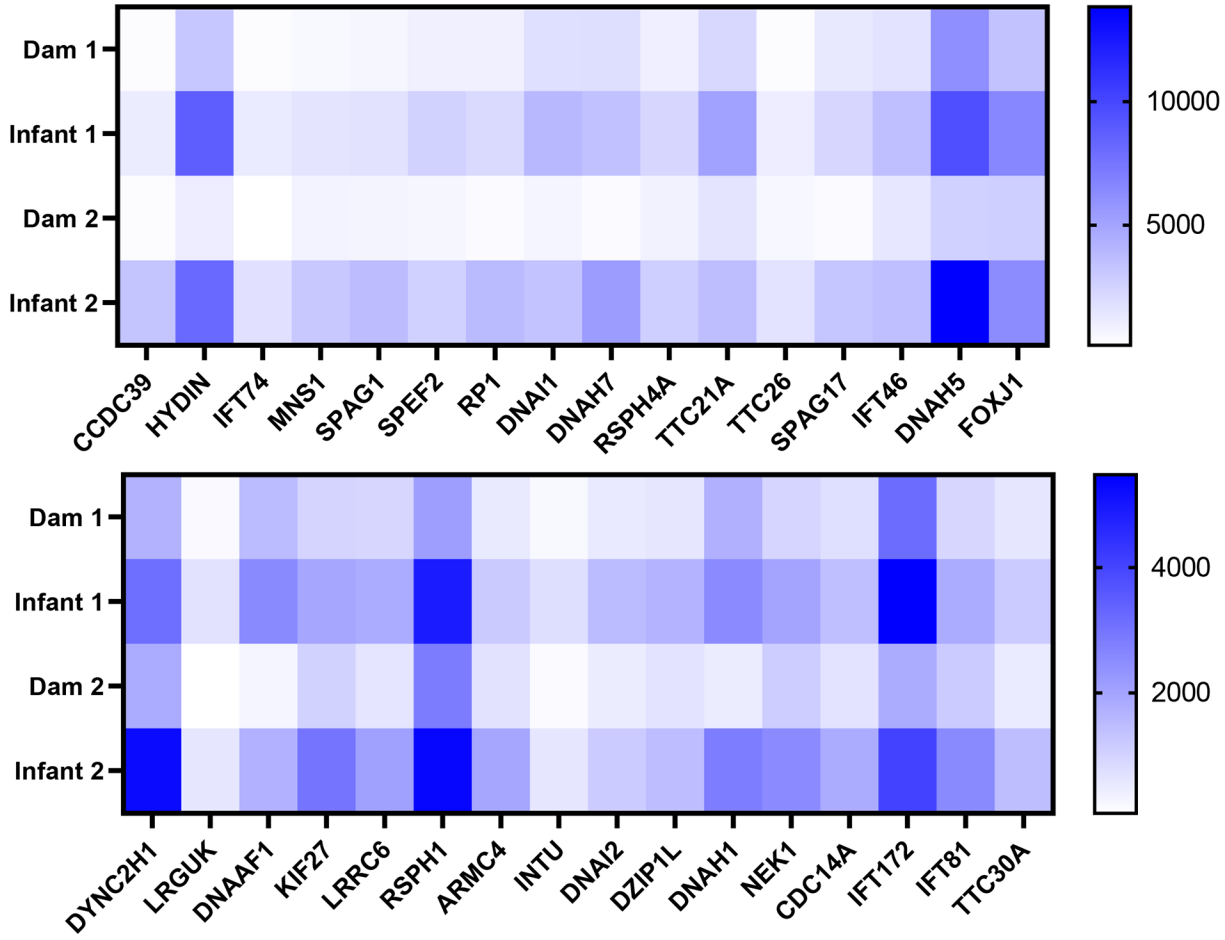

FIG 5.

Age-dependent differences in transcriptomic responses in the trachea reveal cilia injury signatures in adult macaques. (A) Top five out of twenty significantly enriched gene ontology pathways (GO) among downregulated genes in adult compared with infant macaques 14 days after SARS-CoV-2 infection. (B) Heat maps of significantly differentially expressed cilia structure and function-related genes from the *Cilium Organization* GO pathway. Blue represents relative upregulation of gene expression and white represents relative downregulation of gene expression. Genes are arranged by $\log_2$ fold change with the largest $\log_2$ fold change to the left and the smallest $\log_2$ fold change to the right.

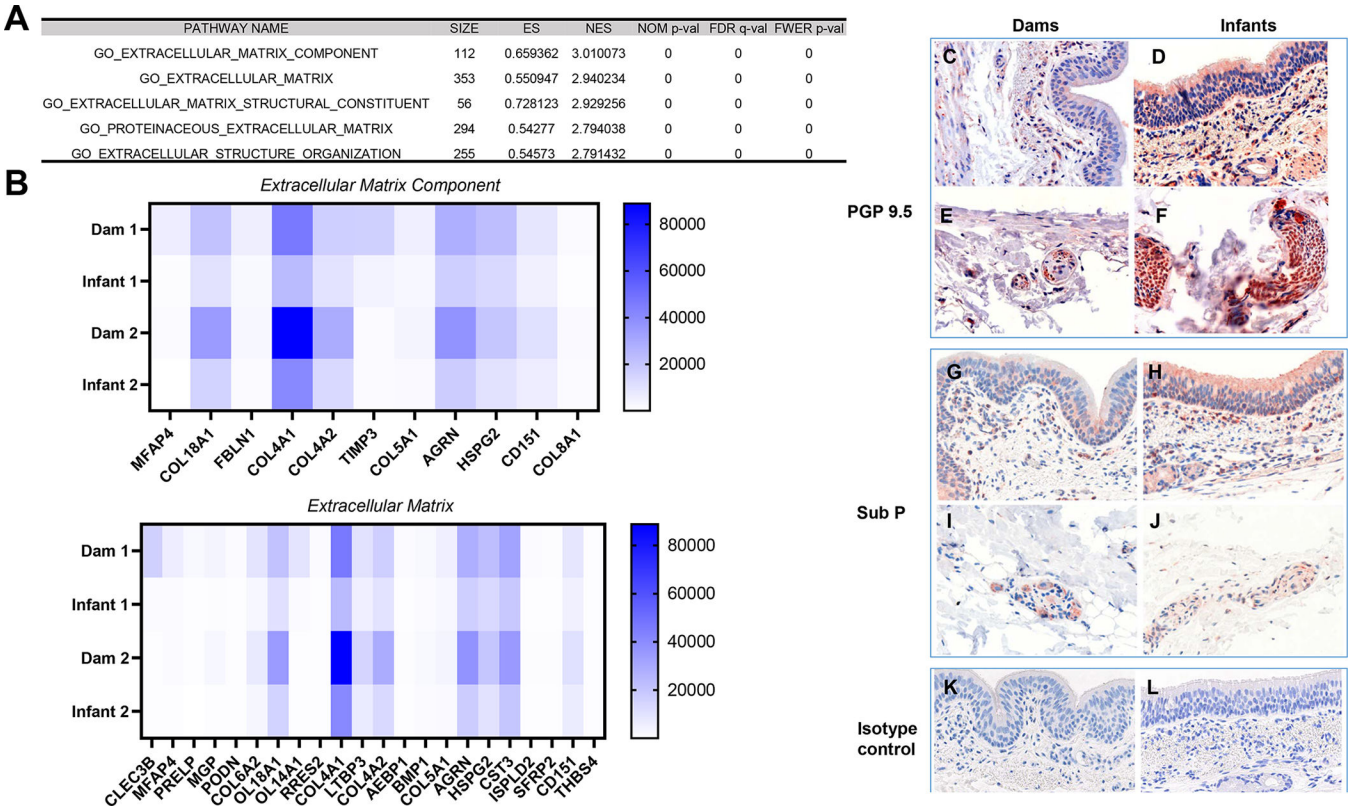

FIG 6.

Upper airways of SARS-CoV-2 infected adult macaques have a profibrotic transcriptomic signature (A) Top five out of thirty-nine significantly enriched gene ontology (GO) pathways among upregulated genes in adult compared with infant macaques 14 days after SARS-CoV-2 infection. (B) Heat map of significantly differentially expressed genes from the *Extracellular Matrix Component* and *Extracellular Matrix* GO pathways. Assessment of protein gene product (PGP) 9.5 expression in (C) dam 1, (E) dam 2, (F) infant 1 and (D) infant 2, substance P (sub P) expression in (G) dam 1, (I) dam 2, (J) infant 1 and (H) infant 2 trachea tissues and (K) dam and (L) infant isotype controls via immunohistochemical staining.